

Optical Torque Sensors for Local Impedance Control Realization of an Anthropomorphic Robot Arm

Dzmitry Tsetserukou, Riichiro Tadakuma, Hiroyuki Kajimoto and Susumu Tachi

The University of Tokyo
7-3-1 Hongo, Bunkyo-ku, Tokyo, 113-8656, Japan.
Email: dima_teterukov@ipc.i.u-tokyo.ac.jp

We recently developed an optical torque sensor to replace expensive strain-gauge-based sensor on the anthropomorphic robot arm and realize local impedance control in individual joints.

Keywords: Optical torque sensor, Impedance control.

1. Introduction

Teleoperated slave robot developed for delicate tasks such as interaction with users in remote environments or manipulation of objects under hazardous conditions¹⁾ includes anthropomorphic seven-degree-of-freedom (7-DOF) arms (Fig. 1) with 8-DOF hands. Impedance control is used to achieve stable environmental interaction and to realize controlled dynamic interaction between a robot arm and users. Impedance control used in the arm of the remote slave robot requires measurement of external force exerted by users during interaction. The force imparted by users on the anthropomorphic arm is measured by a 6-axis force/torque sensor (MINI 4/20, BL AUTOTEC), marked by rectangles in Fig. 1.

Even though the robotic system ensures safe interaction at the end-effector, other parts such as the shoulder and elbow may cause injury during use because they do not have force measurement sensors to limit the motor torque by feedback. Direct sensing of applied torque through the DC motor circuit is not acceptable due to low backdrive in harmonic drives with high gear ratio (≈ 50). To realize user-friendly interaction of

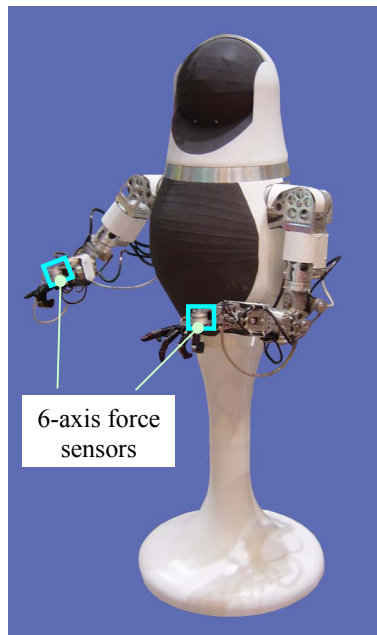


Fig. 1. Teleoperated slave robot.

any part of the anthropomorphic arm, we decided to use torque sensors at each joint to implement local impedance control, achieving virtual backdrive of transmission in each joint.

Commercial 6-axis strain-gauge-based force/torque sensors are used at the end-effector of a robot to monitor assembly or machining. This application requires very high stiffness, but for users-robot interaction, high stiffness is not the objective. Strain gauges have disadvantages of being difficult to install and calibrate, easy to break, and having high electrical noise sensitivity that makes them rather expensive.

We introduce an optical approach to detect torque and discuss the results of local impedance control on the basis of developed optical sensors to provide safety in user-robot interaction.

2. Background

The torque transducer on the motor shaft includes a load cell structure supporting the load and deflecting a known amount in response to applied torque. Deformation of the elastic element is measured in different ways as follows:

- 1) *Electrically*
- 2) *Based on electromagnetic phenomena*
- 3) *Optically*

These approaches include noncontact transducers measuring relative displacement by light radiation detection, Hall effect, Faraday's law, and contacting transducers measuring strain based on strain gauges, potentiometers, piezoelectric, and optical fibre.

2.1. Electrical Methods

Electrical measurement is associated essentially with strain gauges and capacitive and piezoelectric sensing. Strain gauge operation is based on variations in electrical resistance with strain. When force is applied, strain changes the electrical resistance of gauges proportional to the load. Silicon semiconductor strain gauges are often used due to high sensitivity. Strain in silicon causes its bulk resistance to change, producing a signal 75 times stronger than conventional foil gauges where resistance changes are only due to dimensional changes in the resistor. Despite such benefits of strain gauges as high accuracy (linearity), about 0.03%-2.5% of full scale (FS), high resolution of 1-3mV/V, their maximum allowable strain is close to their breaking point. To guarantee

overload protection of transducers, mechanical stops limiting deflections of flexures are necessary. Very stiff sensors may only deflect a few ten-thousandths of a millimeter. Manufacturing limit stops with such small clearances is very difficult. Strain-gauge-based torque/force sensors are greatly subjected to radial and other force components. Semiconductor and foil gages require elaborate process for attachment by a specialist. Another shortcoming of these sensors is their high sensitivity to electrical noise and temperature²⁾.

Piezoelectric torque sensors are similar in operation to strain gauges and based on the phenomenon in which a crystal under the action of mechanical stress becomes electrically charged. High stiffness and strength enable sensors to be directly inserted into the torsion member. An example of the piezoelectric effect is the invention³⁾ where author exploited changes in the resonant frequency of the piezoelectric element as a measure of the strain to which the torsion member is subjected. Extremely high accuracy (0.03% of full scale) and high signal output are their main advantages. Drawbacks restricting their application are high cost and nonlinear output.

Many torque transducers are based on measuring the relative angle between the two ends of the torsion bar. This principle was realized in the differential capacitive sensor for measuring the relative angle⁴⁾. The transducer is noncontact, robust, and compact. Two rotatable electrodes are placed between two sensor plates. The relative angle between the two rotors and the absolute position of the rotor blades are calculated from measurement of capacitive coupling between different transmitting stator segment and a single receiving electrode. Its drawback is high sensitivity to radial displacement and high cost. The relationship between the capacitor capacity and permittivity of the dielectric material between the capacitor plates also was used in patent⁵⁾. In this invention, the apertured metal cage shielding a dielectric rotor is placed between capacitor plate rings fixed on opposite sides of a torsion bar. The relative rotation of the apertured conductive plates and the dielectric rotor changes the overall differential capacitance of the system in proportion to torque.

2.2. Electromagnetic Phenomena

Faraday's law (inductive sensors), magnetostriction, and magnetoelastic effect are used in electromagnetic sensors. The main advantage of linear variable differential transformers (LVDT) is their high degree of robustness, remarkable resolution of about $0.1\mu\text{m}$, good accuracy (0.01-0.3%), and easier installation and calibration. High reliability is derived from their operation principle based on magnetic transfer eliminating physical contact across the sensing element. The strong relationship between core position and output voltage of secondary coils yields excellent resolution. Inductive sensors suffer a reduction in signal at very low frequencies and affected by electromagnetic noise. D. Vischer and O. Khatib used this transducer in the torque sensor⁶⁾. The hub-spoke structure of this torque sensor is given in Fig. 2 (1 – flexible beam, 2 – LVDT).

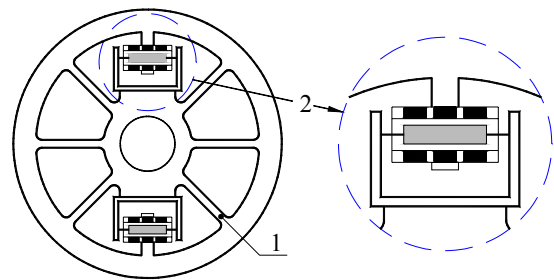


Fig. 2. Six-beam torque sensor with LVDT transducer⁶⁾.

The smallest LVDT made by the Lucas Schaevitz XS-B series weighs only 4.36 g and has an outer diameter of 4.77 mm, but its length of 22.4 mm complicates compact overall dimensions of the torque transducer.

The effect, in which applying stress to the material causes a change in its magnetization, is known as the Villari effect or magnetostriction phenomena. Magnetostrictive torque sensors consist of rotational shaft, having a magnetostrictive metal layer of a chevron configuration formed on the shaft, an exciting coil, and a pickup coil for detecting the magnetic property change of the magnetostrictive layer. When AC current is applied to the exciting core, the magnetostrictive layer is excited. Torque applied to the magnetostrictive element generates stress. Permeability is changed by the Villari effect and inductive output is generated in the pickup coil with torsional load⁷⁾. Advantages of the sensor are no physical contact between the shaft and housing, and high torsional stiffness. Drawbacks are complicated manufacturing, bulky heavy structure, need for a robust magnetic shield, and insufficient performance (linearity – 3-5% FS, hysteresis 2-3%, resolution 10 mV/V)⁸⁾.

2.3. Optical Approaches

A light source, photosensor, and solid object modifying the amount of light incident on the optical detector are necessary to measure displacement between unmovable and flexible parts of the optical sensor. Photosensors have such drawbacks as nonlinearity and temperature sensitivity, but are considerably more reliable, cheap, and simplified in design. A displacement is detected by interrupting light between source and detector, changing the intensity of reflected light, or the relative movement of source and detector. S. Hirose and K. Yoneda have significantly contributed to research on the optical force/torque sensors [9, 10]. They proposed using a split photosensor to detect displacement of the light source (LED) caused by applied force in two directions. This sensor is shown in Fig. 3 (1 – force loaded adapter plate, 2 – load cell (elastic element), 3 – photodetector, 4 – LED, 5 – installation adapter plate).

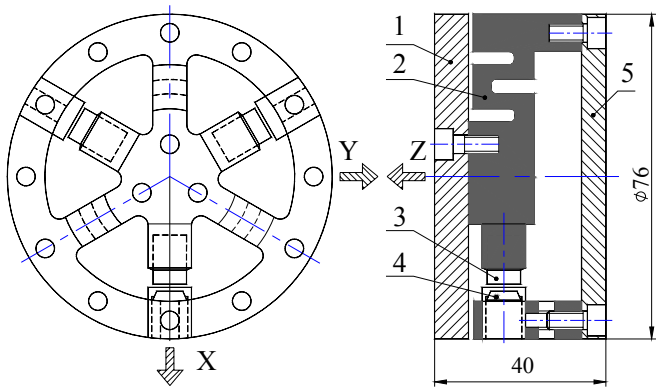


Fig. 3. Layout of the 6-axis optical force/torque sensor⁹⁾.

As force applied to the plate 1, elastic solid body 2 deflects LED light incident on photosensor 3. Thus, magnitude of photodetector output responds on exerting force/moment. In cooperation with the Minebea Co. OPFT series of 6-axis optical force/torque sensors was manufactured. Compared to conventional strain-gauge-based transducers, they are more compact, lightweight, and cheap¹¹⁾, but they have complicated calibration due to nonlinear output, require application of DSP for real-time computation of measured force, and have an average accuracy of 5%.

At Nara Institute of Science and Technology, a 6-axis optical force/torque sensor was developed for fMRI application. The sensor was made from acrylic resin to eliminate any metal sensor components that generate fMRI signal noise. The layout of the transducer¹²⁾ is shown in Fig. 4.

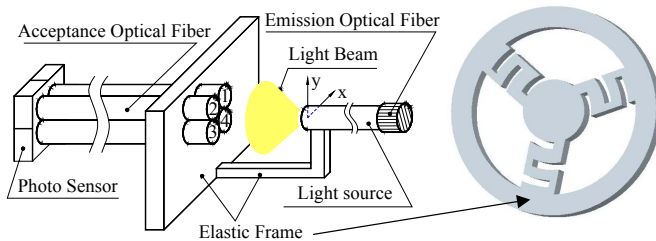


Fig. 4. Layout of the 6-axis optical force/torque sensor¹²⁾.

The elastic frame has a Y-topology with S-shaped beams to enable 6-DOF displacement of the sensing face. Force exerted by users deflects the elastic frame, altering the intensity of light falling on optical fiber. The sensor provides accuracy of 2.65% for measurement of moment M_z . The transducer is complicated and intended only for narrow applications.

The idea of the patent¹³⁾ is calculating torque by measuring the angle of twist of the torsion shaft through detection of differences in the rotation position of disks at opposite sides of the torsion shaft using an optical encoder. The encoder-type torque sensor suffers from large overall dimensions and precise relative installation of apertured disks. To overcome this, the author¹⁴⁾ invented a torque sensor including a source of optical radiation, a two-dimensional

array of a radiation detector and two modulating apertured disks placed between the source and detector. As torque applied to the shaft the relative position between disks alters overlapping slots and hence the size of the apertures which control the pattern of light incident upon the optical detector. The 6-axis force/torque converter using LEDs and photodiodes is given in reference¹⁵⁾.

3. Development of Optical Torque Sensor

3.1. Specifications

Above-mentioned sensors have not been adapted to application in robot for joint torque detection. New slave arm enabling to build in torque sensors is being developed. The 3D model of anthropomorphic robot arm and shoulder with built-in torque sensors is shown in Fig. 5.

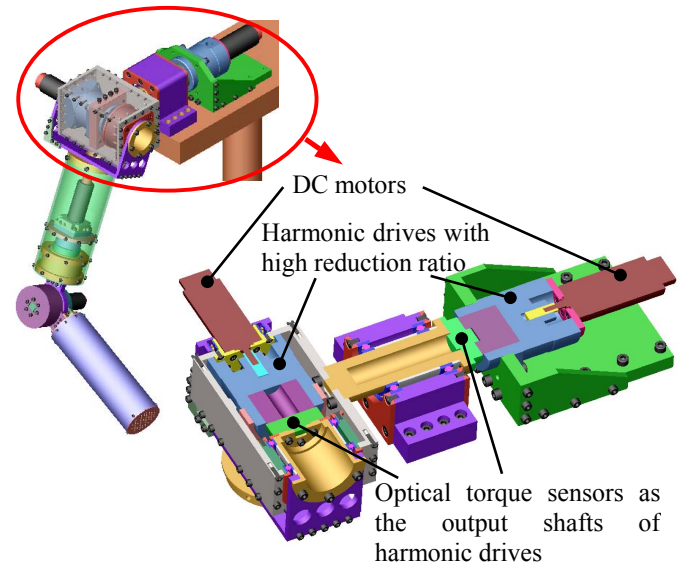


Fig. 5. 3D model of the new anthropomorphic robot arm.

The approach to designing a high-performance torque sensor for the anthropomorphic robot arm should follow the guidelines below.

1. Addition of the torque sensor to a robot joint should not require redesign of the joint and should cause minimal modification in kinematics and dynamics. A sensor with small width and lightweight is desirable.
2. Noise created by current passing through the DC motor at each joint of the robot arm should not affect the sensing element and use of electromagnetic sensors should be avoided in this application.
3. The angle of twist of the movable part of the transducer at the maximum expected external torque should enable exploiting as wide a range of detector sensitivity as possible to achieve high signal-to-noise ratio.
4. Torsional stiffness of the sensor should not considerably reduce the natural frequency of the robot arm. This introduces the trade-off of stiffness maximization while maintaining high sensitivity.
5. The other difficulty in design of the torque sensor is hysteresis elimination. Most metals used as flexures have very

little hysteresis. Bolted, press fit and welded joints near the flexure introduce hysteresis. Optimal design requires realization of the mechanical structure from a single piece of metal.

6. Influence from any of the nontorsional components of load should be canceled to guarantee precise measurement of torque T that is moment around Z -axis M_Z in 6-axis sensors.

7. Behavior of the sensing element output and mechanical structure should be as close to linear as possible.

8. Simple to manufacture, low-cost, and robust.

3.2. Development of New Torque Sensors

We decided to use ultra-small photointerrupters RPI-131 and RPI-121 as sensitive elements to measure the relative motion of sensor components. The relationship between the output signal and position of the shield plate for RPI-121¹⁶⁾ is shown in **Fig. 6**. The linear section of the diagram corresponding to 0.2 mm is used for detection of the relative displacement of the object. The dimensions of the photointerrupter (RPI-121 $3.6 \times 2.6 \times 3.3$ mm) and weight of 0.05 g enable realization of compact sensor design.

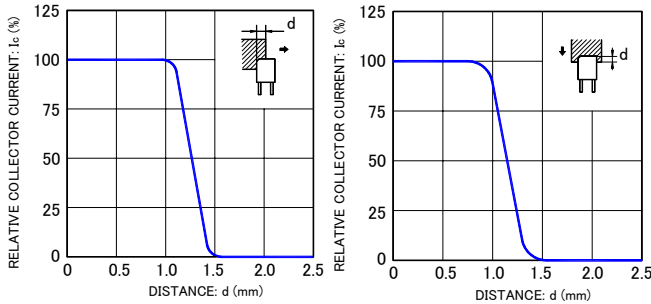


Fig. 6. Relative output vs. distance¹⁶⁾.

Two elastic elements were realized to optimize the sensor design: the in-line structure – when detector input and output are displaced axially by the torsion component and the “in plane” one – when sensor input and output are disposed in one plane and linked by bending radial flexures. The layout of the in-line structure based on a spring with a cross-shaped cross section is shown in **Fig. 7**. This spring enables large deflections without yielding. The detector consists of input part 1, output part 2, fixed photointerrupters 3, shield 4, and cross-shaped spring 5. The operating principle is as follows: when torque T is applied to the input shaft, the spring is deflected, rotating the shield 4. Shield displacement is detected by the degree of interruption of infrared light falling on the phototransistor. The magnitude of the photointerrupter output signal corresponds to applied torque. The “in plane” arrangement of the load cell was

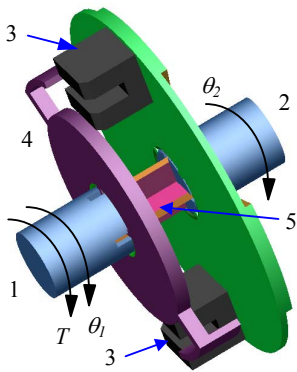


Fig. 7. Construction of the optical torque sensor.

The operating principle is as follows: when torque T is applied to the input shaft, the spring is deflected, rotating the shield 4. Shield displacement is detected by the degree of interruption of infrared light falling on the phototransistor. The magnitude of the photointerrupter output signal corresponds to applied torque. The “in plane” arrangement of the load cell was

designed to decrease the thickness of the transducer. The layout of the structure having hub and three spokes (Y-shaped structure) and adjustment mechanism of shield plate is shown in **Fig. 8**.

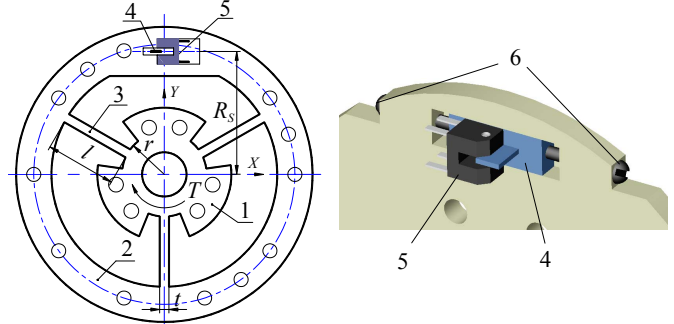


Fig. 8. Layout of Y-shaped spring and position regulator.

The detector consists of inner part 1 connected by flexure 3 with outer part 2, fixed photointerrupter 5, slider with shield plate 4, and screws 6. When torque is applied, radial flexures are bent. The shield is adjusted by rotating oppositely located screws 6. The pitch of screws enables smooth movement of the slider with the shield plate. The relationship between the sensed torque T_S and the angle of twist θ is linear:

$$T_S = k_S \theta = k_S (\theta_1 - \theta_2), \quad (1)$$

where k_S – torsional stiffness of flexure (Nm/rad).

Hub rigidity is increased by introducing additional evenly distributed spokes¹⁷⁾. The torsional stiffness of this sensor is derived from:

$$k_S = 4NEI \left(\frac{1}{l} + \frac{3r}{l^2} + \frac{3r^2}{l^3} \right), \quad (2)$$

where N – number of spokes, l – the spoke length, E – modulus of elasticity, r – inner radius of the sensor⁶⁾. The moment of inertia of spoke cross section I is calculated as:

$$I = \frac{bt^3}{12}. \quad (3)$$

Here b – beam width, t – beam thickness. The sensor was designed to withstand torque of 0.8 Nm. The results of analysis using FEM show von Mises stress in MPa under a torque T of 0.8 Nm (**Fig. 9a**), tangential displacement in mm (**Fig. 9b**), von Mises stress under a bending moment M_{YZ} of 0.8 Nm (**Fig. 9c**), and von Mises stress under an axial force F_Z of 10 N (**Fig. 9d**).

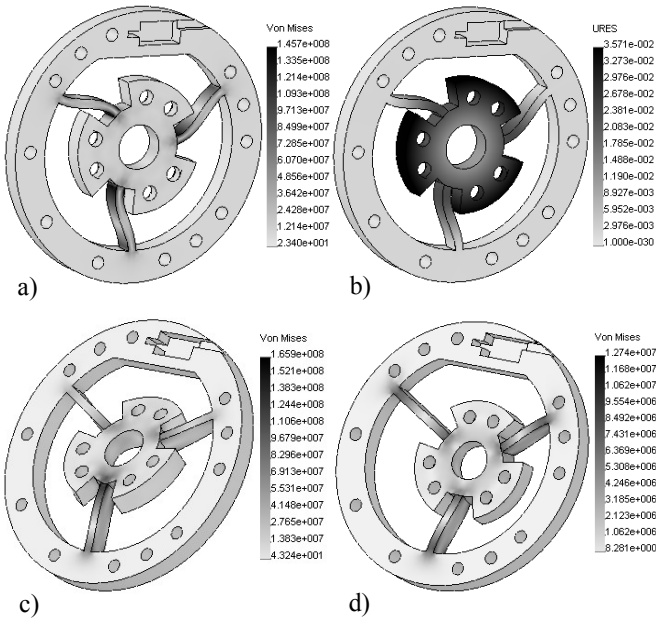


Fig. 9. Results of analysis using FEM.

The maximum von Mises stress under torque T of 0.8 Nm equals $\sigma_{MaxVonMises} = 14.57 \cdot 10^7 \text{ N/m}^2 < \sigma_{yield} = 15.0 \cdot 10^7 \text{ N/m}^2$. The angle of twist of 0.209° is calculated from the tangential displacement. The ability to counteract bending moment is estimated by the coefficient:

$$K_{TM} = \frac{\sigma_{MaxVonMises}(T)}{\sigma_{MaxVonMises}(M_{YZ})} \quad (4)$$

Y-shaped spring coefficient $K_{TM} = 0.878$. The same approach to estimate the ability to counteract axial force F_Z is applied:

$$K_{TF} = \frac{\sigma_{MaxVonMises}(T)}{\sigma_{MaxVonMises}(F_Z)} \quad (5)$$

After substitution of magnitudes, we calculate $K_{TF} = 11.44$. Our sensor was machined from one piece of brass using wire electrical discharge machining (EDM) cutting to eliminate hysteresis and guarantee high strength (Fig.10). In this sensor, the ultra-small photointerrupter RPI-121 is used. The sensor is only 6.5 mm thick.



Fig. 10. Optical torque sensor with hub-spoke-shaped flexure.

In the test rig for calibrating the optical sensor (Fig.11), force applied to the arm, secured by screws to the rotatable shaft, creates the loading torque. Calibration was realized by incrementing the angle of twist with small steps and measuring the output signal from the photointerrupter.

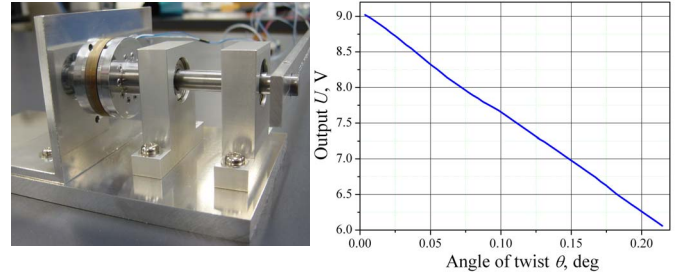


Fig. 11. Test rig and calibration result.

The ring-shaped spring was designed to extend the exploiting range of photodetector sensitivity while keeping same strength and outer diameter. Components and assembly of the developed optical torque sensor are shown in Fig. 12 (1 – shield plate, 2 – photointerrupter RPI 131, 3 – ring-shaped flexure). The flexible ring is connected to the inner and outer part of the sensor through beams. Inner and outer beams are displaced with an angle of 90° that enables large compliance of the ring-shaped flexure.

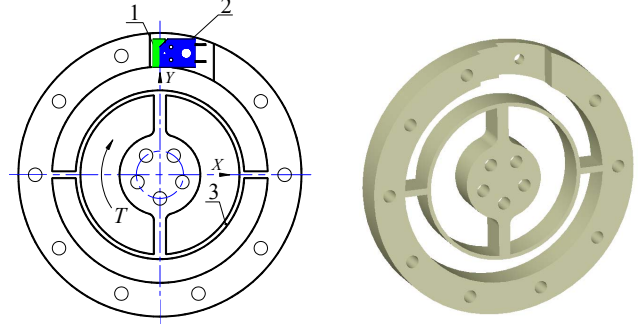


Fig. 12. New topology and 3D model.

The results of analysis using FEM show von Mises stress in MPa under torque T of 0.8 Nm (Fig. 13a), tangential displacement in mm (Fig. 13b), von Mises stress under bending moment M_{YZ} of 0.8 Nm (Fig. 13c), and von Mises stress under axial force F_Z of 10 N (Fig. 13d).

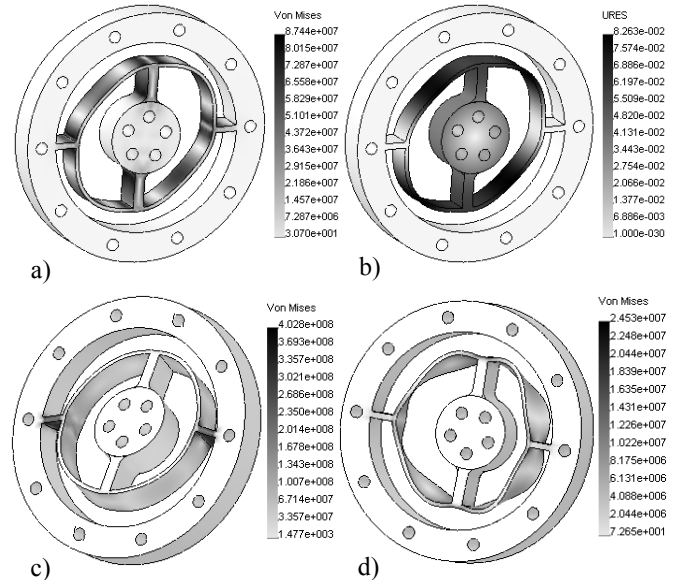


Fig. 13. Result of analysis using FEM.

The maximum von Mises stress under torque T of 0.8 Nm equals $\sigma_{MaxVonMises} = 8.74 \cdot 10^7 \text{ N/m}^2 < \sigma_{yield} = 8.96 \cdot 10^7 \text{ N/m}^2$. Given structure provides the following coefficients $K_{TM} = 0.217$, $K_{TF} = 3.56$ and angle of twist θ of 0.4° . Thus, the ring-shaped structure enables magnifying the angle of twist deteriorating degree of insensitivity to bending torque and axial force. This structure was machined from one piece of aluminium A5052. The components and assembly of the optical torque sensor are shown in Fig. 14. The sensor is 10 mm thick. The displacement of the shield is measured by photointerrupter RPI-131. The shortcomings of this design are complicated procedure of adjusting the position of the shield relatively photosensor and deficiency of the housing to prevent from damage of the optical transducer.

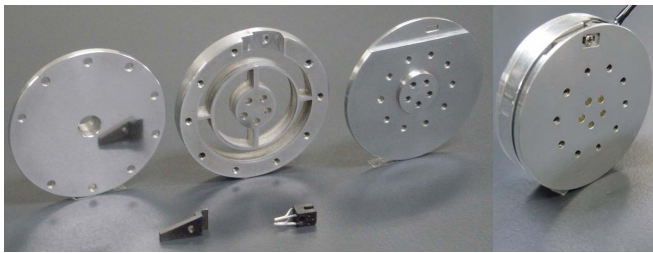


Fig. 14. Optical torque sensor with ring-shaped flexure.

The setup in Fig. 11 was used to calibrate the sensor. The relationship between angle of twist θ and the output voltage of photointerrupter is shown in Fig. 15.

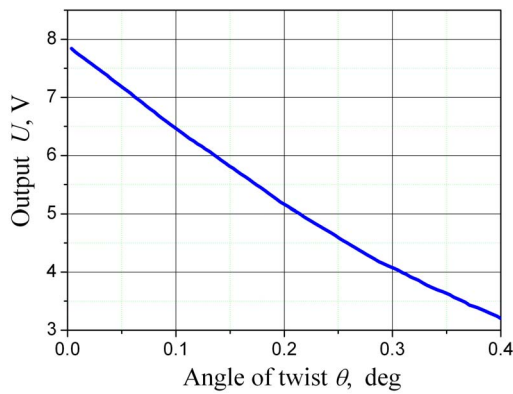


Fig. 15. Calibration result.

The sensor with a ring topology was modified. The layout of the detector with semicircular flexure and 3D model are given in Fig. 16 (1 – shield, 2 – photointerrupter RPI 131, 3 – semicircular flexure).

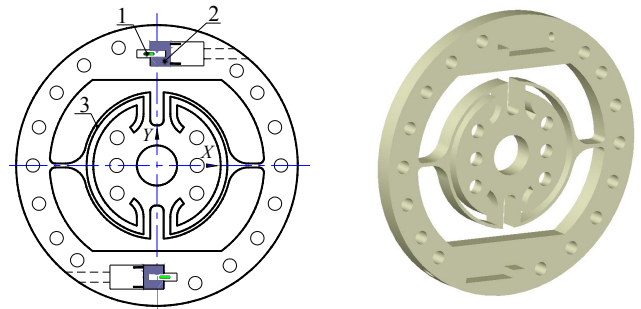


Fig. 16. Semi-ring-shaped spring.

The results of analysis using FEM show von Mises stress in MPa under torque T of 0.8 Nm (Fig. 17a), tangential displacement in mm (Fig. 17b), von Mises stress under bending moment M_{YZ} of 0.8 Nm (Fig. 17c), and von Mises stress under axial force F_Z of 10 N (Fig. 17d).

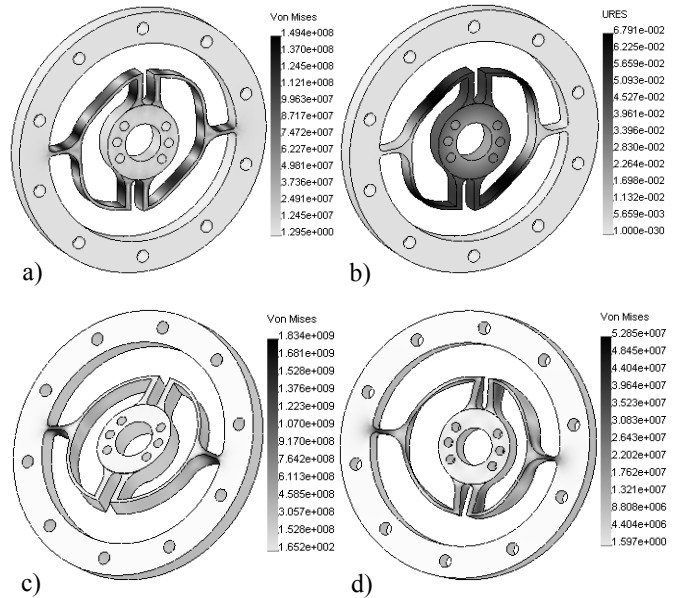


Fig. 17. Results of analysis using FEM.

The maximum von Mises stress $\sigma_{MaxVonMises} = 14.94 \cdot 10^7 \text{ N/m}^2 < \sigma_{yield} = 15.0 \cdot 10^7 \text{ N/m}^2$. The semicircular flexure provides the following coefficients $K_{TM} = 0.082$, $K_{TF} = 2.83$ and angle of twist θ of 0.39° . This structure was machined from one piece of brass C2801. Components and assembly of this optical torque sensor are shown in Fig. 18.



Fig. 18. Optical torque sensor with semi-ring-shaped flexure.

The sensor is 7.5 mm thick. Its drawback is high sensitivity to bending moment. The relationship between angle

of twist θ and the output voltage is shown in **Fig. 19**.

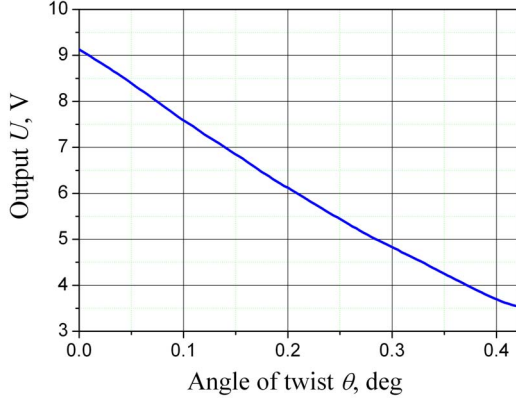


Fig. 19. Calibration result.

Technical specifications of optical torque sensors are listed in **Table 1**.

Table 1. Technical specifications

Sensor	Hub-spoke spring	Ring-shaped spring	Semicircular spring
Spring member material	Brass C2801	Aluminium A5052	Brass C2801
Photointerrupter type	RPI-121	RPI-131	RPI-121
Load capacity, Nm	0.8	0.8	0.8
Torsional stiffness, Nm/rad	219.8	115.86	116.99
Natural frequency, kHz	5.25	2.7	1.37
Factor of safety	1.0	1.0	1.0
Outer diameter, mm	42	42	42
Thickness, mm	6.5	10.0	7.5
Sensor mass, g	34.7	28.7	36.8

The technical specifications of 6-axis force/torque sensors with a similar sensing range of torque around Z-axis are listed in **Table 2** [11,18,19].

Table 2. Technical specifications of 6-axis force sensors

Sensor	ATI Mini 40 Y-shaped beam	BL Autotec Mini 2/10 Y-shaped beam	Minebea OPFT-50N Y-shaped beam
Spring member material	Hardened stainless steel	Stainless steel	Aluminium
Sensing element	Silicon strain gauge	Strain gauge	LED-Photodetector
Sensing range M_z , Nm	1.0	1.0	2.5
Torsional stiffness Z-axis, Nm/rad	4300		
Natural frequency, kHz	3.2		
Accuracy, %		1.0	5.0
Factor of safety	5.0	5.0	1.5
Outer diameter, mm	40	40	50
Thickness, mm	12.25	20	31.5
Sensor mass, g	50	90	133

The spoke-hub topology enables a compact sensor. The

large torsional stiffness diminishes photointerrupter resolution. The semicircular spring has high sensitivity to bending moment and axial force and small natural frequency. The optimal solution is the ring-shaped flexure providing wide torsional stiffness with high mechanical strength. The main shortcoming of this topology is high sensitivity to bending moment. Nevertheless, this obstacle is overcome through realization of a simple supported loading shaft of the robot joint. In most loaded joints, e.g. shoulder, such material as hardened stainless steel can be used for elastic elements to keep sensor dimensions. Our optical sensors compared to strain-gauge-based sensor ATI Mini 40 have small torsional stiffness and low factor of safety. Nevertheless such advantages as low cost, easy manufacture, and compactness make them preferable for torque measurement in robot arm joints. The linear transfer characteristic of the photointerrupter simplifies calibration of the sensor.

4. Local Impedance Control

The objective of impedance control is to establish the dynamic relationship between position error and force error in interaction similar to Newton's second law of motion. The graphical presentation of local impedance control is given in **Fig. 20**.

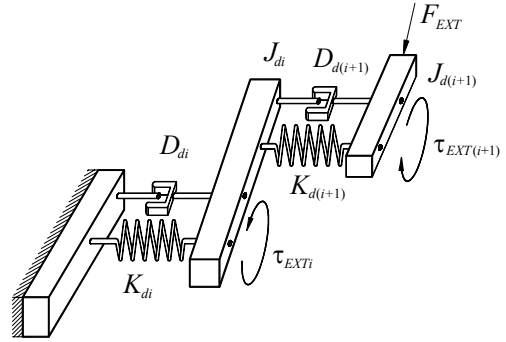


Fig. 20. Concept of the local impedance control.

In joint space desired dynamics of robot joint i is:

$$\tau_{EXTi} = J_{di} \Delta \ddot{\theta}_i + D_{di} \Delta \dot{\theta}_i + K_{di} \Delta \theta_i; \Delta \theta_i = \theta_{ci} - \theta_{di}, \quad (6)$$

where τ_{EXTi} – torque applied to joint i caused by external force F_{EXT} , J_{di} – desired inertia, D_{di} – desired damping, K_{di} – desired stiffness, θ_{ci} – output joint angle of the impedance model, θ_{di} – desired joint angle. The state-space presentation of the equation of local impedance control is written:

$$\begin{bmatrix} \Delta \dot{\theta}_i \\ \dot{v}_i \end{bmatrix} = \begin{bmatrix} 0 & 1 \\ -K_d/J_d & -D_d/J_d \end{bmatrix} \begin{bmatrix} \theta_i \\ v_i \end{bmatrix} + \begin{bmatrix} 0 \\ 1/J_d \end{bmatrix} \tau_{EXTi}(t), \quad (7)$$

where the state variable is defined as $v_i = \Delta \dot{\theta}_i$.

After integration of (7), the discrete time presentation of the impedance equation is expressed as:

$$\begin{bmatrix} \Delta \theta_{k+1} \\ \Delta \dot{\theta}_{k+1} \end{bmatrix} = A_d \begin{bmatrix} \Delta \theta_k \\ \Delta \dot{\theta}_k \end{bmatrix} + B_d T_{EXT(k)}. \quad (8)$$

where A_d and B_d – matrixes mapped by discretization, $T_{EXT(k)}$ – measured external torque. To verify the dynamic behavior of the optical torque sensors, the local impedance control of links of a simple SCARA manipulator was implemented (Fig.21, torque sensors are marked by ovals). Speed reducers with gear ratios of 2548 were selected to guarantee very low backdriving of joints.

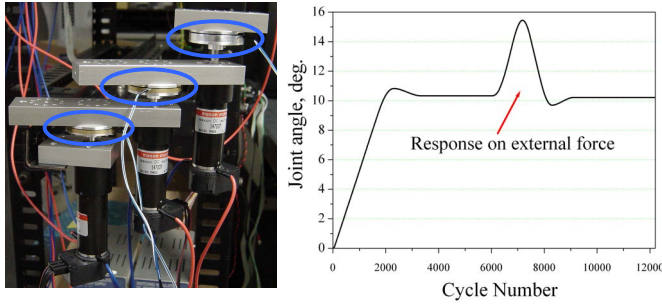


Fig. 21. SCARA type manipulator.

The position-based local impedance control is shown in Fig. 22 (K_p and K_D – proportional and derivative feedback gains). The second-order low-pass filter was implemented to eliminate the noise component with a cutoff frequency of 80 Hz.

5. Conclusions

New optical torque sensors to replace the strain-gage-based 6-axis force/torque sensor and realize virtual backdrivability of joint transmissions have been developed. These sensors are compact, lightweight, easy to manufacture, and have good linearity, enough resolution, and electromagnetic noise immunity. Position-based local impedance control of a SCARA manipulator has been successfully implemented. Real-time computation of inverse dynamics of the robot is not required that greatly decrease computation time. The new anthropomorphic arm with ability to build in developed torque sensors has been designed. New research will realize of the local impedance control of each joint of the anthropomorphic robot arm which precise 3D drawings using CAD is shown in Fig. 5. When torque sensors

are placed coaxially with joint axes, they will be subjected to gravitational force of neighboring links. This will also be included in our future work.

References:

- 1) R. Tadakuma, Y. Asahara, H. Kajimoto, N. Kawakami, and S. Tachi: "Development of Anthropomorphic multi-D.O.F. Master-slave Arm for Mutual Telexistence," *IEEE Transactions on Visualization and Computer Graphics*, vol. 11, no. 6, pp. 626-636, November 2005
- 2) J. D. Turner and M. H. Westbrook, *Automotive Sensors*. Bristol, U.K.:IOP, 1993.
- 3) J. A. Kovacich et al., "Method of Manufacturing a Piezoelectric Torque Sensor," U.S. Patent 6 442 812 B1, 2002.
- 4) P. L. Fulmek, F. Wandling, W. Zdiarsky, G. Brasseur, and S. P. Cermak, "Capacitive Sensor for Relative Angle Measurement," *IEEE Transactions on Instrumentation and Measurement*, vol. 51, no. 6, pp. 1145-1149, December 2002.
- 5) A. M. Madni, R. K. Hansen, and J. B. Vuong, "Differential Capacitive Torque Sensor," U.S. Patent 6 772 646, 2004.
- 6) D. Vischer and O. Khatib, "Design and Development of High-performance Torque Controlled Joints," *IEEE Transactions on Robotic and Automation*, vol. 11, no. 4, pp. 537-544, August 1995.
- 7) O. Shinoura, "Torque Sensor and Manufacturing Method of the Same," U.S. Patent 6 574 853 B2, 2003.
- 8) R. Ishino et al., "Magnetostrictive Torque Sensor Shaft," U.S. Patent 5 491 369, 1996.
- 9) S. Hirose and K. Yoneda, "Robotic Sensors with Photodetecting Technology," *Proc. of 20th International Symposium on Industrial Robotics*, pp. 271-278, 1989.
- 10) S. Hirose and K. Yoneda, "Development of Optical 6-axis Force Sensor and its Non-linear Calibration," *J. of RSI*, vol.8-25, pp.19-28, 1990.
- 11) Minebea, "6-Axial Force Sensor," Minebea Co., Ltd., [Online], Available: <http://www.minebea-mcd.com/6-axial/index.htm>.
- 12) N. Takahashi et al., "An optical 6-axis Force Sensor for Brain Function Analysis using fMRI," *Proc. of 2nd IEEE International Conf. On Sensors*, vol. 1, pp. 253-258, October 2003.
- 13) N. Okutani and K. Nakazawa, "Torsion Angle Detection Apparatus and Torque Sensor," U. S. Patent 5 247 839, 1993.
- 14) S. J. Horton, "Displacement and Torque Sensor," U. S. Patent 6 800 843 B2, 2004.
- 15) A. J. Hilton, "Force and Torque Converter," U. S. Patent 4 811 608, 1989.
- 16) Photointerrupter Design Guide. *Product catalog of ROHM*, pp. 6-7, 2005.
- 17) C. Nicot, "Torque Sensor for a Turning Shaft," U. S. Patent 6 694 828 B1, 2004.
- 18) ATI, "Multi-Axis Force/Torque Sensor," ATI Industrial Automation, [Online], Available: http://www.ati-ia.com/library/documents/ATI_FT_Sensor_Catalog_DE_C2005.pdf
- 19) BL AUTOTEC, "BL Sensor," BL AUTOTEC, LTD., [Online], Available: <http://www.bl-autotec.co.jp/english/pdf/bl-sensor.pdf>.

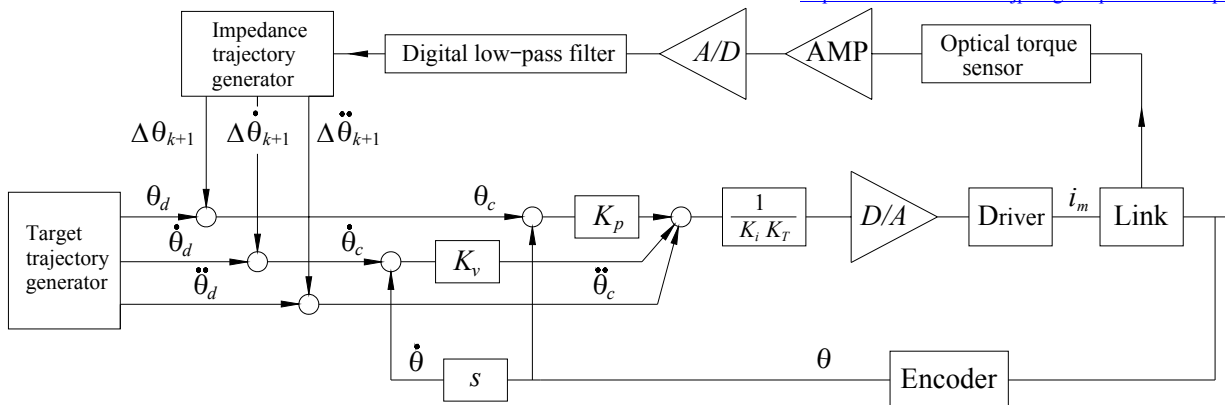


Fig. 22. Block diagram of position based local impedance control system.